IEEE International Conference on Robotics & Automation (San Francisco, CA)
April 22-28, 2000

# Isotropy and Actuator Optimization in Haptic Interface Design

S. E. Salcudean and L. Stocco

Department of Electrical and Computer Engineering
The University of British Columbia, Vancouver, British Columbia, Canada V6T 1Z4
tims@ece.ubc.ca, leos@ece.ubc.ca

## Abstract

*A haptic interface controlled in impedance mode should present its user with a uniform force capability matching the human hand. This paper reviews a mechanism design methodology that maximizes a workspace-inclusive isotropy index. Force maximization in coreless or voice-coil motors is also considered in order to maximize haptic interface acceleration. Example designs of a planar 3-DOF haptic mouse, a 5-DOF haptic pen and a MagLev joystick are presented.*

## 1 Introduction

Research in haptic interfaces has led to a number of novel devices that have been used in demonstrations, teleoperation and training. Design criteria have included low effective mass [11], low variations in mass [5], [13], [14], kinematic isotropy [10], [24], stability robustness [2] and a large workspace [8]. Iwata [6] built a 9-DOF Compact Master which combines a 6-DOF parallel positioning device in series with three 1-DOF finger actuators. Iwata [7] also used a pair of commercial 3-DOF hybrid manipulators to actuate each end of a 6-DOF haptic pen. In [1], the 6-DOF hybrid SMARTee interface uses a parallel combination of three 2-DOF serial linkages. In [3], a 6-DOF joystick is described which contains three pantograph linkages and Yokoi *et. al.* [23] presents a 6-DOF serial hand controller with three prismatic actuators for translation and three rotary actuators for orientation. A 5-DOF (3 translation, 2 rotation) haptic stylus is described in [12] which uses 5 linear actuators in parallel. A 4-DOF (3 translation, 1 rotation) hybrid device using rotary actuators is presented in [9] while a 4-DOF Manipulandum that combines a 3-DOF planar parallel robot in series with a linear vertical motion stage is described in [15]. The hybrid PHANToM of [14] has three active translational degrees of freedom and three passive rotational degrees of freedom. A 2-DOF planar pantograph is optimized in [5] and the 2-DOF linear voice coil actuated Magic Mouse is presented in [8]. Finally, Vertut [22] presents a historical survey of earlier hand controllers, articulated arms and exoskeletons.

Most of the interfaces described above have been developed as part of demonstration systems to evaluate potential applications of haptic interfaces, control algorithms and human factors, with relatively little attention paid to the optimization of electromechanical characteristics. In this paper we make the argument that force isotropy over a workspace is a useful and computationally tractable performance criterion for haptic interface design. Following a discussion of design criteria, we outline a previously developed design methodology to achieve force isotropy and present four design examples, a 2-DOF planar pantograph, a planar 3-DOF dual pantograph with unlimited rotation range, a 5-DOF haptic pen and a 6-DOF magnetically levitated interface. We then illustrate how voice-coil or coreless motors can be optimized for maximum force (given power) or acceleration in haptic interfaces. Acceleration has been argued to be extremely important in a number of studies [5], [17]. This is primarily a survey paper, with the only previously unreported work being the 3-DOF twin pantograph design.

## 2 Design Criteria

Many design specifications are relevant to the performance of a haptic interface. They include workspace size, position bandwidth, force magnitude, force bandwidth, velocity, acceleration, effective mass, accuracy, and so on. A survey of proposed values for many of these design specifications can be found in [19]. Most of these values are derived from the inherent capabilities of a human hand since this the environment of a haptic interface.

A haptic interface presents an impedance which is varied in an intelligent fashion to simulate different environments. Two types of devices can be used to implement an intelligent variable impedance, an impedance device and an admittance device. An impedance device is easily backdriveable in its passive state and typically uses direct drive or moderately geared actuators to adjust its effective impedance by applying a force based on position and velocity. An admittance device is the dual of an impedance device. It is not backdriveable in its passive state and typically uses highly geared actuators to adjusts its effective impedance by inducing motion based on applied force.

The high inertia and friction that exists in a highly geared admittance device inhibits high frequency transitions (i.e. switching between free motion and hard contact) and is difficult to actively compensate resulting in low transparency and sluggish free motion that can be tiring during prolonged use. Therefore, we are more interested here in design issues related to impedance devices.

As discussed by Colgate and Schenkel [2], it is difficult to actively compensate for the physical dynamics of a mechanical system without compromising stability. Therefore, a haptic device's minimum impedance is decreased by a reduction in mechanical impedance. Salcudean and Vlaar [17] also show that even when high static forces are not available, high stiffnesses can be simulated by inducing high acceleration. Therefore, it follows that both high and low impedance emulation are improved and the impedance range is widened when mechanical impedance is reduced. Reducing mechanical impedance can be done in a number of ways that do not necessarily involve kinematic design and the mass matrix. It may, in fact, be sufficient to use a parallel device, light weight materials, low friction joints and counterbalances so that kinematic design can be focussed on other criteria such as force.

If an impedance device's mechanical impedance is sufficiently small, its performance is dictated by its force capabilities. Since actuators can always be scaled to meet any force magnitude requirements, it does not make much sense to maximize force through kinematic design. It is more practical to focus instead on isotropy. Since a device is only as good as its worst-case performance inside its workspace, improving isotropy strengthens its weaknesses and allows smaller actuators to be used. This results in lower rotor inertia, consistently stiff virtual environments, improved compactness and lower cost. Force isotropy is achieved by making the Jacobian transpose $J^T(p,x)$ (for a parallel manipulator) isotropic.

## 3 Design Approach

For the robot designs presented here, static force isotropy is optimized through kinematic design. First a condition index is formulated which evaluates a device's performance as a function of its design parameters. Then, an optimization algorithm is used to select the design parameters that produce the best result. The Global Isotropy Index proposed in [20] is used to evaluate the isotropy of a performance matrix. Physical units are normalized and the GII is adjusted to evaluate performance with respect to a direction dependent specification as a function of geometric and actuator scale parameters by the technique described in [21]. The design parameters which maximize the GII are found using the culling algorithm which is described in [20]. The culling algorithm is a discrete optimization algorithm that is specifically designed to handle GII and minimax problems. It can be used with any performance function, places no limitation on the number of free variables, is insensitive to initial conditions and guarantees the same result as a global search but finds it orders of magnitude faster.

The 6×6 Jacobian force/torque transformation shown in (1) is normalized to remove physical units and scaled to account for task-space requirements and actuator capabilities in (2) using the scaling matrices $S_J$ and $S_T$ in (3) and (4) where $\tau_1$ through $\tau_6$ are maximum actuator torques and $F$ and $M$ are maximum force and moment requirements along axes $i$, $j$ and $k$. The GII is computed in (5) from the minimum $\underline{\sigma}(\hat{J}(p, x_0))$ and maximum $\tilde{\sigma}(\hat{J}(p, x_1))$ singular values of the normalized Jacobian $\hat{J}(p, x)$ evaluated for a design parameter $p$ at all positions $x_0$, $x_1$ inside the workspace $W$. The culling algorithm is used to solve the optimization problem in (6) for the parameter $p^*$ that maximizes the global isotropy index $GII(p)$ where $p$ is a design parameter belonging to the set of candidates $P$.

$$f = J(x)^T \tau \tag{1}$$

$$\hat{J}(x) = S_J J(x) S_T^{-1} \tag{2}$$

$$S_J = Diag\left(\begin{bmatrix}\tau_1 & \tau_2 & \tau_3 & \tau_4 & \tau_5 & \tau_6\end{bmatrix}\right) \tag{3}$$

$$S_T = Diag\left(\begin{bmatrix}F_i & F_j & F_k & M_i & M_j & M_k\end{bmatrix}\right) \tag{4}$$

$$GII(p) = \min_{x_0, x_1 \in W} \frac{\underline{\sigma}(\hat{J}(p, x_0))}{\tilde{\sigma}(\hat{J}(p, x_1))} \tag{5}$$

$$p^* = \arg\max_{p \in P} \left(GII(p)\right) \tag{6}$$

## 4 Design Examples

The GII and culling algorithm are used to select the design variables for two variations of the Twin-Pantograph haptic interface. The first is a 3-DOF planar haptic mouse and the second is a 5-DOF spatial haptic pen.

### 4.1 Haptic Mouse

The 3-DOF Twin-Pantograph haptic mouse is shown in Figure 1. It uses two 2-DOF 5-bar linkages to translate the journals of a crank-shaft end-effector in the plane, thereby providing two degrees of translation and one degree of rotation. The unique quality of this design is that the rotation range is unlimited. Note that one actuator is redundant and only serves to improve kinematic conditioning (i.e. it removes a singularity) and allows the control of the two pantographs to be decoupled into two 2-DOF positioning devices.

The device is designed to operate within a $100\text{cm}^2$ ($10\text{cm(x)} \times 10\text{cm(y)}$) motion range with infinite rotation. The crankshaft length $l_6$ is first determined as a function of end-effector diameter $l_5$, in order to respect the relative force/torque capabilities of the human hand determined in [21]. For a comfortably sized knob ($l_5=1.25\text{cm}$), $l_6$ is computed from (7) where $f_{max}$ and $\tau_{max}$ are the maximum force and torque capabilities of the human hand for planar

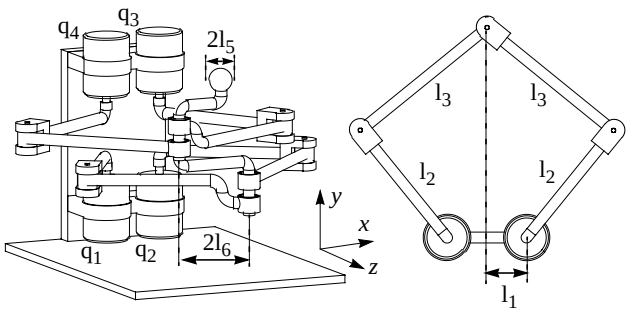


Figure 1: 3-DOF Twin-Pantograph Haptic Mouse

motions and *d* is the diameter of the rod that was used in the biomechanics experiment.

$$l_6 = \frac{2\tau_{max}}{d f_{max}} l_5 = 1.6 l_5 \quad (7)$$

Next, the geometries of the pantographs are taken from the results presented in [20]. In [20], the static force isotropy of a single pantograph was repeatedly optimized for a *10*cm square workspace whose centre was positioned from *30*cm below to *30*cm above the base link ($l_1$ in Figure 1). The optimum geometries and static force GII are plotted against workspace placement in Figure 2.

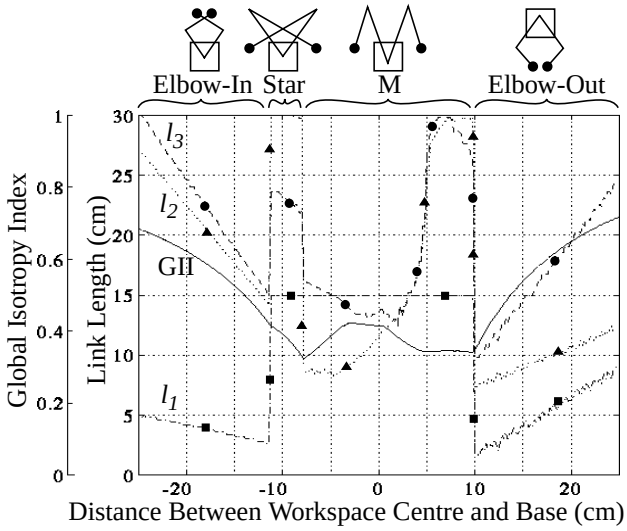


Figure 2: Optimum 5-Bar Linkage Geometries

The values in Figure 2 are scaled to correspond to a larger workspace (original workspace augmented on all four sides by the radius of the crankshaft $l_6$) and are used to select the link lengths of the haptic mouse.

Mass is minimized by using aluminum clevises, carbon fibre links and low inertia, rare earth magnet Maxon motors. Friction and backlash are minimized by using direct drive motors and roller bearings in all of the passive joints. The position of each active joint is sensed by a *1000* window (*4000*cpt) optical encoder. A photograph of the device is shown in Figure 3.

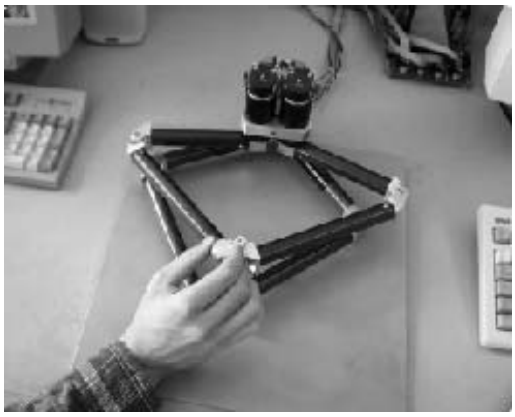

Figure 3: The Twin-Pantograph Haptic Mouse

Measured performance values for the Twin-Pantograph haptic mouse are reported in Table 1. All values correspond to the robot at its home position. The stiffness and damping coefficients are obtained by tuned PD control at a control rate of *500*Hz with the end-point velocity computed from low-pass filtered finite difference position readings. The minimum force is the force required to overcome static friction and the dynamic range is the ratio between the minimum and peak force/torque capabilities.

**Table 1: Haptic Mouse Performance Specifications**

| | Translation Axis | | Rotation (y-axis) |
|---|---|---|---|
| | x | z | |
| Workspace (cm) | ±5 | ±5 | ∞ |
| Spatial Res (μm) | 224 | 224 | 0.26˚ |
| Min F/T (N,Ncm) | 0.024 | 0.024 | 0.12 |
| Cont F/T (N,Ncm) | 2.4 | 2.26 | 12 |
| Peak F/T (N,Ncm) | 23 | 22 | 115 |
| Dyn Range | 950:1 | 910:1 | 950:1 |
| Eff Mass (g,gcm$^2$) | 395 | 370 | 4781 |
| Peak Accel (G,s$^{-2}$) | 6 | 6 | 2405 |
| Max Stiff (N/cm,Ncm) | 25 | 25 | 200 |
| Max Damp (Ns/cm,Nscm) | 0.7 | 0.7 | 5 |

By comparison, the 3-DOF SensAble PHANToM haptic interface is cited in [14] to have a spatial resolution of *64*μm, a continuous force of *1.5*N, a dynamic range of *100:1*, a tip inertia of *100*g and a maximum stiffness of *35*N/cm. However, since there is no standard method for making these measurements, the cited values may not be entirely comparable.

See [18] for a discussion on the approach taken to control the Twin-Pantograph haptic mouse and [4] for a discussion on the haptic rendering of the virtual slave that was tele-operated by the Twin-Pantograph haptic mouse.

### 4.2 Haptic Pen

The 5-DOF Twin-Pantograph haptic pen is shown in Figure 4. It uses two 3-DOF 5-bar linkages that are actuated about their folding or waist joints ($q_1$, $q_4$) to provide three degrees of translation and two degrees of rotation to a pen shaped end-effector. As in the case of the haptic mouse, one actuator is redundant but serves to remove a singularity and decouple the controller. The sixth degree of freedom (roll about the pen axis) is passive. This device lends itself well to applications which do not rely on reaction torques from axial rotations.

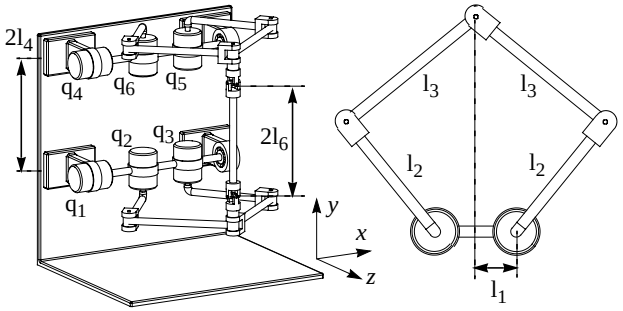


Figure 4: 5-DOF Twin-Pantograph Haptic Pen

The device is designed to operate within a $1600\text{cm}^3$ ($16\text{cm(x)} \times 10\text{cm(y)} \times 10\text{cm(z)}$) motion range with a $\pm 45^\circ$ rotation range. Since isotropy is improved by moving the workspace further from the base, the optimization problem is solved for a range of reasonable workspace positions ($15$cm - $40$cm). Increasing the base length ($l_4$) also improves isotropy since it distances the workspace from the actuators so $l_4$ is made equal to $l_6$. The resulting device has 5 free design parameters which are shown with the optimal solutions in Table 2 where $Q_1$ is the relative waist:shoulder actuator torque ratio. Note that $l_1$ is assigned a minimum value of $2.4$cm to account for the width of the shoulder actuators and $l_6$ is assigned a minimum length of $7.0$cm so that the end-effector can be held comfortably by a human hand.

**Table 2: Effect of Workspace Position on GII**

| Dist | $l_1$ | $l_2$ | $l_3$ | $l_6$ | $Q_1$ | GII |
|---|---|---|---|---|---|---|
| 15cm | 2.4 | 13.0 | 16.0 | 7.0 | 1.6 | 0.089 |
| 20cm | 2.4 | 14.5 | 20.0 | 7.0 | 1.7 | 0.182 |
| 25cm | 2.4 | 17.0 | 23.0 | 7.0 | 1.6 | 0.234 |
| 30cm | 3.6 | 19.5 | 27.0 | 7.0 | 1.6 | 0.262 |
| 35cm | 3.6 | 22.5 | 30.5 | 7.0 | 1.6 | 0.280 |
| 40cm | 4.0 | 25.5 | 34.5 | 7.0 | 1.6 | 0.292 |

Since isotropy significantly degrades below $20$cm and improvements become marginal above $25$cm, the prototype Twin-Pantograph haptic pen is built with its workspace $20$cm from the base. It uses motors, clevises, bearings, linkage material and position sensors that are similar to those used in the previous design. Gravitational effects are minimized by steel counterbalances mounted behind the shoulder motors and larger actuators are used at the waist joints to satisfy the additional torque requirements. A photograph of the device is shown in Figure 5.

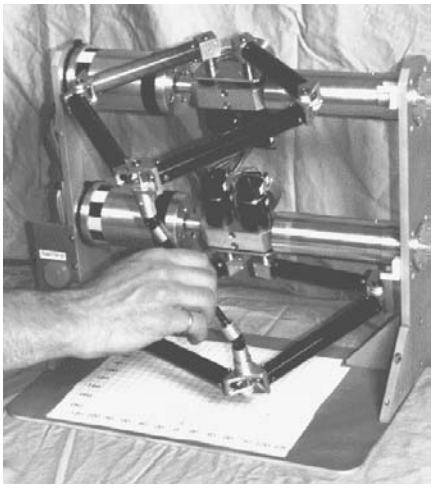

Figure 5: The Twin-Pantograph Haptic Pen

Measured performance values for the Twin-Pantograph haptic pen are reported in Table 3. All values correspond to the robot at its home position except for unbalanced weight which is a workspace inclusive range. The stiffness and damping coefficients are obtained by tuned PD control at a control rate of $1$kHz. Other values are measured the same as for the haptic mouse.

**Table 3: Haptic Pen Performance Specifications**

| | Translation Axis | | | Rotation Axis | |
|---|---|---|---|---|---|
| | x | y | z | x | z |
| Workspace (cm) | ±6 | ±3.75 | ±3.75 | ±45˚ | ±45˚ |
| Spatial Res (μm) | 247 | 314 | 247 | 0.173˚ | 0.173˚ |
| Min F/T (N,Ncm) | 0.022 | 0.045 | 0.023 | 0.19 | 0.18 |
| Cont F/T (N,Ncm) | 2.5 | 3.3 | 2.0 | 17 | 21 |
| Peak F/T (N,Ncm) | 24 | 21 | 20 | 162 | 198 |
| Dyn Range | 1100:1 | 480:1 | 860:1 | 860:1 | 1100:1 |
| Eff Mass ($g,gcm^2$) | 190 | 226 | 156 | 10300 | 12600 |
| Peak Accel ($G,s^{-2}$) | 13 | 10 | 13 | 1574 | 1573 |
| Max Stiff (N/cm,Ncm) | 16 | 12 | 13 | 874 | 1076 |
| Max Damp (Ns/cm,scm) | 0.44 | 0.5 | 0.36 | 24 | 30 |
| Weight (g) | 70 - 130 | | | | |

## 5 PowerMouse Electro-Mechanical Design

A desk-top magnetically levitated haptic interface called PowerMouse has been developed and is described in [16].

The device has six degrees of freedom, high acceleration, but limited motion range. Its electromechanical design is summarized in this section. As seen in Figure 6, the device has a handle attached to a cubic "flotor" structure with the flat coils of six Lorentz actuators embedded in its faces. Twenty-four magnets on a stator structure generate the six magnetic fields that cross the coils. The wide magnetic gaps of the Lorentz actuators allow six-degree-of-freedom (6-DOF) motion of the flotor, with a motion range of ±3mm and ±5˚ from a nominal center.

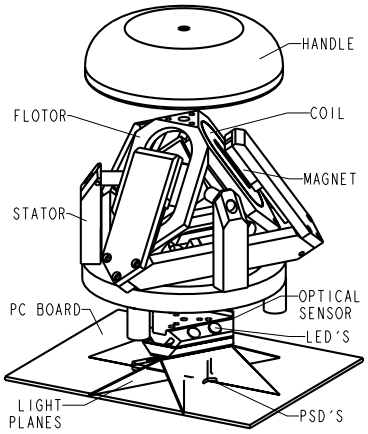


Figure 6: PowerMouse Mechanical Design

An optical 6-DOF sensor detects the flotor motion with three LED-generated infrared light planes projected in sequence on three linear position sensing diodes (PSDs), mounted as an equilateral triangle on the PowerMouse printed circuit (PC) board. Each light plane crosses two PSDs. Thus six light-plane intersections with PSDs are obtained, allowing for the solution of the handle location using a direct kinematics computation.

The actuators have been optimized to maximize the force to power consumption ratio. It has been experimentally verified that, as a result of the optimized actuators, the device operates far below its limits suggesting that a larger workspace could be obtained by increasing the magnetic gaps.

The mapping from voice-coil actuator currents to the force-torque vector acting on the flotor of the device is isotropic by design, featuring two sets of equal singular values, one corresponding to force, the other to torque. The relative strength of forces and torques can be determined from biomechanics studies (see, e.g. [21]) and by size requirements. Since the device workspace is small and the generated forces and torques do not vary much with flotor location, there was no need to compute and minimize the device GII. Performance values for the PowerMouse are reported in Table 4.

**Table 4: PowerMouse Performance Specifications**

| | |
|---|---|
| Workspace | ±3mm, ±5˚ |
| Spatial Resolution | 10μm, 0.05˚ |
| Continuous Force | 16N |
| Peak Force | 34N |
| Effective Mass | 260g |
| Peak Acceleration | > 10G |

## 6 Actuator Force Optimization

Commercially available electric motors are not optimized for haptic interfaces. Coreless motors such as those produced by Maxon, Micromo or Bertsch have small inertias and torque ripples but seem to be optimized for efficiency rather than force and work best at high speeds/high transmission ratios. Such motors have been used in a number of reported haptic interfaces (SensAble PHANToM [14], Hayward *et. al.* Pantograph [5]). We present here an approach to optimize actuator force per unit power. Without loss of generality, we consider the flat voice coil actuator shown in Figure 7, but it should be noted that the optimization approach can be applied just as well to conventional coreless DC motors.

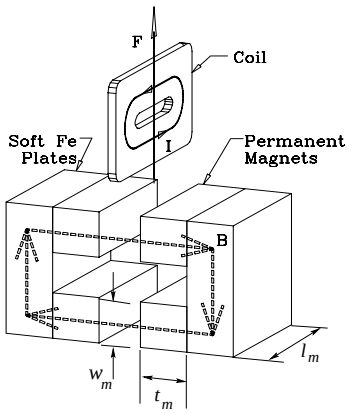


Figure 7: Basic Flat Coil Actuator

Let $d_c$ be the coil width, $d$ the gap between the magnets, and $d_r=d-d_c$ the coil "rattle space" that allows motion in all degrees of freedom, not only in the direction of actuation. Let $l_{wire}$ be the coil wire length, and $\eta_{pack}$ be the coil "packing efficiency", i.e., $\eta_{pack}=s_{eff}/s_{wire}$, the ratio of conducting to total wire cross-sectional area. Note that $\eta_{pack}$ depends on the wire cross-sectional shape (best packing achieved by flat wire), and the ratio of insulating material to conducting material. Let ρ be the coil conductor resistivity and $R$ be the coil resistance. Let $P_{coil}$ be the power dissipated in the coil, and let $I$ be the coil current.

The actuator force is given by Lorentz's law. In obtaining the design formula (8) below, it is assumed that (i) the flux crossing the coil is a constant $B_g$, and, (ii) fringing fields are

negligible, i.e., the flux outside the magnet projection through the coil is negligible. For the actuator in Figure 7, given assumption (ii), the length of wire that produces a force is given by $l_{eff}=2l_m w_m d_c/s_{wire}$. Then, with $\eta_{geom}=2l_m w_m d_c/(s_{wire} l_{wire})$ being an efficiency factor determined by the coil geometry, we obtain the following expression for the actuator force where $l_m$, $w_m$ and $t_m$ are the length, width and thickness of the magnet:

$$F(B_g, d, l_m, w_m, t_m) = B_g I l_{eff} = B_g \sqrt{\frac{P_{coil}}{R}} \frac{2l_m w_m d_c}{s_{wire}} = B_g \sqrt{\eta_{pack}} \sqrt{\eta_{geom}} \sqrt{\frac{P_{coil}}{\rho}} \sqrt{2 w_m l_m (d - d_r)} \quad (8)$$

For the coil shown in Figure 7, $\eta_{geom} \approx 2l_m w_m/(2l_m w_m + \pi w_m^2)$, and is approximately *0.6*. Packing efficiencies for conventional (round copper wire) coils are about 75%, with flat copper coils reaching values close to 95%. Assuming that the actuator flux in Figure 7 is steered perfectly by the soft iron back-plates, the field in the center of the gap aligned with the center of the magnet can be calculated by replacing the actuator magnets with equivalent solenoids and using the Biot-Savart Law:

$$B_g(d, l_m, w_m, t_m) = \frac{2B_r}{\pi}\left[\tan^{-1}\frac{w_m l_m}{d\sqrt{d^2 + l_m^2 + w_m^2}} - \tan^{-1}\frac{w_m l_m}{(4t_m + d)\sqrt{(4t_m + d)^2 + l_m^2 + w_m^2}}\right] \quad (9)$$

where $B_r$ is the magnetic material residual flux. Substituting (9) in (8), one can relate the actuator dimensions to the resulting force. The thickness of the iron return plates $t_s$ can have an additional lower bound of the form $t_s \geq \alpha w_m$ to avoid saturation. With appropriate inequality constraints to account for the desired geometrical dimensions, e.g., $2t_s+2t_m+d \leq d_{max}$, $t_m$, $w_m$, $l_m$, and $d$ that maximize actuator force can be obtained by solving a nonlinear program. The geometrical efficiency $\eta_{geom}$ increases with the ratio $l_m/w_m$, while $l_m+2w_m$ will be bounded by flotor size. Furthermore, note that the above formulation does not involve the coil resistance, only the power dissipated in it, its resistivity and geometrical properties. Thus the coil resistance can be selected for maximum power transfer from the power amplifier *after* finding its dimensions.

This design procedure was applied to the PowerMouse design. To simplify the optimization, the values for $l_m$, $w_m$ were selected separately as a function of the desired motion and force range and desired force linearity. Then the magnet thickness $t_m$ and the magnetic gap were selected by plotting the actuator force as a function of the magnetic gap $d$ for a number of readily available magnet dimensions, as shown in Figure 8 and choosing the maximizing $d$, i.e., the best coil-width for a given rattle space. By extending the magnetic field formula (9), the field along the magnet center line can be predicted. The predicted curve for the optimal gap (*11*mm) obtained in the maximum force plot in Figure 8 is displayed in the magnetic flux plot in Figure 8. Note that the field increases near the magnets, giving a non-uniform force. This is averaged, to a certain extent, by the thick coil.

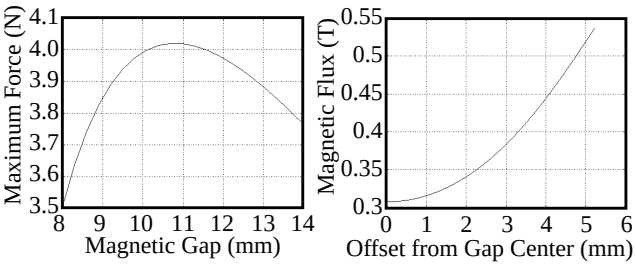


Figure 8: Actuator Force vs Gap with $d_r=6$mm at $P_{coil}=8$W ($l_m=20$mm, $w_m=8$mm and $t_m=4$mm), Giving Actuator Gain at a Current of *1*A and Predicted Gap Field at Optimum Gap (*11*mm)

Relative to prior designs employed by the authors and others, the force for given magnet volume and dissipated power is almost four times larger than in previously reported work on magnetically levitated haptic interfaces. This is largely due to the fact that the coil width to gap ratio is substantially larger than had been used in the past. Predicted force and field values have been compared to experimental ones with small errors (less than 5%) in several voice coil actuator designs of various sizes.

Coreless motor torque could be optimized in a similar manner, combining Lorentz's Law with Biot-Savard's Law to generate a total motor torque as a function of the motor physical parameters. We expect that the rotor thickness would be substantially higher than in present motor designs.

## 7 Conclusion

To ensure comfort during prolonged use, a haptic interface must be able to emulate very low mechanical impedances corresponding to free motion. For emulation of stiff environments, high accelerations are required. Since, in most cases, mass can be optimized by selecting suitable materials and damping can be controlled at the actuator level, the force performance of haptic interfaces is of primary importance in their design.

We have presented an approach to optimize the force isotropy of mechanisms. The force isotropy optimization involves the maximization of a workspace inclusive isotropy measure defined as a function of the haptic interface mechanical parameters. Several design examples have been presented. The force optimization of voice coil actuators or coreless electric motors suitable for parallel or

direct drive devices has also been considered. A simple formulation of force magnitude as a function of motor physical parameters has been proposed and leads to a nonlinear optimization problem that is easily solved. A design example for a voice coil actuator has been presented.

## Acknowledgments

This work is supported by the Canadian IRIS/PRECARN Network of Centres of Excellence. The authors would like to thank Niall Parker, Simon Bachmann and Simon DiMaio for their contributions.

## References

[1] K. Cleary, T. Brooks, "Kinematic Analysis of a Novel 6-DOF Parallel Manipulator", *Proc. IEEE Int. Conf. Robotics & Auto.* (Atlanta, USA), pp. 708-713, May 2-6, 1993.

[2] J.E. Colgate, G.G. Schenkel, "Passivity of a Class of Sampled-Data Systems: Application to Haptic Interfaces", *J. Robotic Sys.*, v. 14, no. 1, pp. 37-47, Jan. 1997.

[3] C.L. Collins, G.L. Long, "The Singularity Analysis of an In-Parallel Hand Controller for Force-Reflected Teleoperation", *IEEE Trans. Robotics & Auto.*, v. 11, no. 5, pp. 661-669. Oct. 1995.

[4] D. Constantinescu, I. Chau, S.P. DiMaio, L. Filipozzi, S.E. Salcudean, F. Ghassemi, "Haptic Rendering of Planar Rigid-Body Motion using a Redundant Parallel Mechanism", *Proc. IEEE Int. Conf. Robotics & Auto.* (San Francisco, USA), Apr. 22-28, 2000.

[5] V. Hayward, J. Choksi, G. Lanvin, C. Ramstein, "Design and Multi-Objective Optimization of a Linkage for a Haptic Interface", *Proc. ARK '94, 4th Int. Workshop on Adv. in Robot Kin.* (Ljubliana, Slovenia), pp. 352-359, June 1994.

[6] H. Iwata, "Artificial Reality with Force-Feedback: Development of Desktop Virtual Space with Compact Master Manipulator", *SIGGRAPH* (Dallas, Texas), v. 24, no. 4, pp. 165-170, Aug. 6-10, 1990.

[7] H. Iwata, "Pen-based Haptic Virtual Environment", *IEEE Int. Symp. Virtual Reality* (Seattle, Washington), pp. 287-292, 1993.

[8] A.J. Kelley, S.E. Salcudean, "The Development of a Force-Feedback Mouse and its Integration into a Graphical User Interface", *Proc. Int. Mech. Eng. Cong. & Expo.* (Chicago, Illinois), DSC-Vol. 55-1, pp. 287-294, Nov. 6-11, 1994.

[9] T. Kotoku, K. Komoriya, K. Tanie, "A Force Display System for Virtual Environments and its Evaluation", *IEEE Int. Workshop on Robot & Human Comm.* (Tokyo, Japan), pp. 246-251, Sept. 1-3, 1992.

[10] R. Kurtz, V. Hayward, "Multiple-Goal Kinematic Optimization of a Parallel Spherical Mechanism with Actuator Redundancy", *IEEE Trans. Robotics & Auto.*, v. 8, no. 5, pp. 644-651, Oct. 1992.

[11] D.A. Lawrence, J.D. Chapel, "Performance Trade-Offs for Hand Controller Design", *Proc. IEEE. Int. Conf. Robotics & Auto.* (SanDiego, California), pp. 3211-3216, May 1994.

[12] C.D. Lee, D.A. Lawrence, L.Y. Pao, "Guaranteed Convergence Rates for Five Degree of Freedom In-Parallel Haptic Interface Kinematics", *Proc. IEEE Int. Conf. Robotics & Auto.* (Detroit, Michigan), pp. 3267-3274, May 10-15, 1999.

[13] O. Ma, J. Angeles, "Optimum Design of Manipulators Under Dynamic Isotropy Conditions", *Proc. IEEE Int. Conf. Robotics & Auto.* (Atlanta, Georgia), pp. 470-475, (May 2-6, 1993).

[14] T.H. Massie, J.K. Salisbury, "The PHANToM Haptic Interface: A Device for Probing Virtual Objects", *Proc. Int. Mech. Eng. Congress & Exposition* (Chicago, USA), Vol. DSC-Vol. 55-1, pp. 295-301, Nov. 6-11, 1994.

[15] P.A. Millman, M. Stanley, J.E. Colgate, "Design of a Four Degree-of-Freedom Force-Reflecting Manipulandum with a Specified Force/Torque Workspace", *Proc. IEEE Int. Conf. Robotics & Auto.* (Sacramento, California), pp. 1488-1493, Apr. 9-11, 1991.

[16] S.E. Salcudean, N.R. Parker, "6-DOF Desk-Top Voice-Coil Joystick'', *6th Annual Symposium on Haptic Interfaces for Virtual Environments and Teleoperation Systems, Intl. Mech. Eng. Congr. Exp., ASME WinterAnnual Meeting* (Dallas, Texas), DSC-Vol. 61, pp. 131-138, Nov. 16-21, 1997.

[17] S.E. Salcudean, T.D. Vlaar, "On the Emulation of Stiff Walls and Static Friction With a Magnetically Levitated Input/Output Device", *Trans. ASME - J. Dyn. Sys. Meas. & Cont.*, v. 119, no. 1, pp. 127-132, Mar. 1997.

[18] M.R. Sirouspour, S.P. DiMaio, S.E. Salcudean, P. Abolmaesumi, C. Jones, "Haptic Interface Control - Design Issues and Experiments with a Planar Device", *Proc. IEEE Int. Conf. Robotics & Auto.* (San Francisco, USA), Apr. 22-28, 2000.

[19] L. Stocco, S.E. Salcudean, "A Coarse-Fine Approach to Force-Reflecting Hand Controller Design", *Proc. IEEE Int. Conf. Robotics & Auto.* (Minneapolis, Minnesota), v. 1, pp. 404-410, Apr. 22-28, 1996.

[20] L. Stocco, S.E. Salcudean, F. Sassani, "Fast Constrained Global Minimax Optimization of Robot Parameters", *Robotica, Int. J. Info., Edu. & Res. in Robotics & Art. Intell.*, v. 16, pp. 595-605, 1998.

[21] L.J. Stocco, S.E. Salcudean, F. Sassani, "On the Use of Scaling Matrices for Task-Specific Robot Design", *IEEE Trans. Robotics & Auto.*, v. 15, no. 5, pp. 958-965, Oct. 1999.

[22] J. Vertut, "Control of Master Slave Manipulators and Force Feedback", *Proc. 1977 Joint Auto. Control Conf.*, 1977.

[23] H. Yokoi, J. Yamashita, Y. Fukui, M. Shimojo, "Development of 3D-Input Device for Virtual Surface Manipulation", *3rd IEEE Int. Workshop on Robot & Human Commun.* (Nagoya, Japan), pp. 134-139, July 18-20, 1994.

[24] K.E. Zanganeh, J. Angeles, "Kinematic Isotropy and the Optimum Design of Parallel Manipulators", *Int. J. Robotics Res.*, v. 16, no. 2, pp.185-197, Apr. 1997.